Controlling second coordination sphere effects in heterogeneous catalysis

A molecular approach

Laan, P.C.M.

Publication date
2024

Chapter 3

Non-covalent Grafting of Molecular Complexes to Solid Supports by Counterion Confinement

Part of this work has been published as:

Non-covalent Grafting of Molecular Complexes to Solid Supports by Counterion Confinement

P. C. M. Laan, E. O. Bobylev, N. J. Geels, G. Rothenberg, J. N. H. Reek, N. Yan

J. Phys. Chem. C **2023**, *127*, 24129-24136.

DOI: 10.1021/acs.jpcc.3c05691

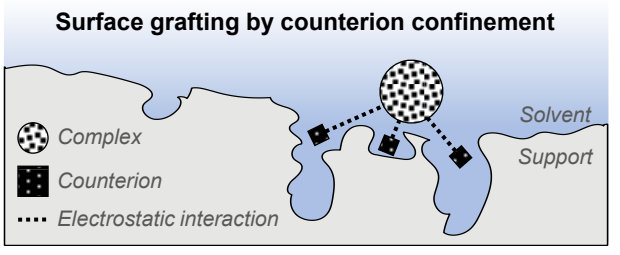

Abstract: Grafting molecular complexes on solid supports is a facile strategy to synthesize advanced materials. Here, we present here a general and simple method for non-covalent grafting on charge-neutral surfaces. Our method is based on the generic principle of counterion confinement in surface micropores. We demonstrate the power of this approach using a set of three platinum complexes: Pt_1 ($Pt_1L_4(BF_4)_2$, L = *p*-picoline), Pt_2 ($Pt_2L_4(BF_4)_4$, L = 2,6-bis(pyridine-3-ylethynyl)pyridine) and Pt_{12} ($Pt_{12}L_{24}(BF_4)_{24}$, L = 4,4'-(5-methoxy-1,3-phenylene)dipyridine). These complexes share the same counterion (BF_4^-) but differ vastly in their size, charge, and structure. Imaging of the grafted materials by aberration corrected high-angle annular dark-field scanning transmission electron microscopy (AC-HAADF-STEM) and energy-dispersive X-ray (EDX) showed that our method results in a homogeneous distribution of both the complexes and counterions. Nitrogen sorption studies indicated a decrease in available surface area and micropore volume, providing evidence for counterion confinement in the surface micropores. Following the adsorption of the complexes over time and showed that this is a two-step process: fast *surface adsorption* by van der Waals forces was followed by migration over the surface and *surface binding* by counterion confinement. Regarding the binding of the complexes to the support, we found that the surface-adsorbate binding constant (K_S) increases quadratically with the number of anions per complex up to K_S = 1.6×10^6 M^{-1} equalling $\Delta G°_{ads}$ = –35 kJ mol^{-1} for the surface binding of Pt_{12}. Overall, our method has two important advantages: first, it is general, as you can anchor different complexes (with different charges, counterions and/or sizes). Second, it promotes the distribution of the complexes on the support surface, creating well distributed sites that can be used in various applications across several areas of chemistry.

Introduction

Addressing today's environmental challenges requires a re-design of the energy and chemical sectors.[1] The rate of this change depends on the development of new functional materials for electrolysers[2], solar-to-fuel processes[3] and metal-air batteries[4]. The energy transition will only take place if we can provide economically viable alternatives.[5] Carbon-based catalytic materials are especially important here, owing to their low cost, high thermal and electrical conductivity, and tuneable surface properties.[6–8]

Advancing these materials further often requires a combination of functionalities, such as catalytic activity and electrical conductivity. This can be done by anchoring molecular complexes on carbon-based supports, most commonly by covalent binding.[9] Yet this method incurs additional steps, increasing the cost and hampering large-scale application. Moreover, the covalent bonds can change the function of the molecular complex, and typically require custom-made solutions for each case.

A much simpler approach is grafting the complexes on surfaces using sorption methods, but these bindings are often too weak.[10] One way to solve this is by immobilization based on electrostatic interactions, where weakly coordinating counterions are exchanged by a charged solid that acts as a "counterion" instead. This method, however, works only for charged supports.[11]

Here we describe a new and general strategy for immobilising molecular species on charge-neutral carbon-based materials. Our concept is based on non-covalent anchoring, by confining the counterions of the complexes in the support pores. We test this concept by immobilizing a series of platinum complexes with varying charges on a porous carbon. The anchored complexes were characterised by aberration corrected high-angle annular dark-field scanning transmission electron microscopy (AC-HAADF-STEM), energy-dispersive X-ray (EDX) imaging and detailed nitrogen sorption studies. Our results show that the counterions are indeed confined in the micropores and that the complexes are evenly distributed over the support. Adsorption kinetics studies showed that this immobilization is a two-step process. Moreover, the adsorption isotherms showed that the binding is stronger as

the number of counterions per complex increases. This general yet simple method opens opportunities for making new functional materials for the energy transition.

Results and discussion

Design and synthesis of the model system

Our hypothesis was that confining the counterions in the surface pores would result in strong binding of the complex to the support surface, especially if three criteria are met: *(i)* the complex has multiple counterions, *(ii)* the counterions fit well in the pores, and *(iii)* additional stabilizing interactions between counterion and pore are possible (**Figure 1**).

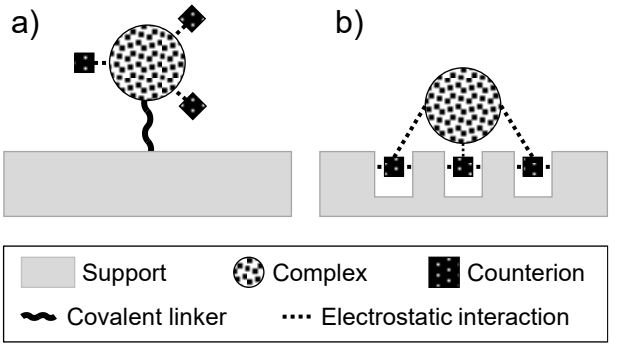

Figure 1. *Methodologies to perform immobilization by a) covalent tethering and b) non-covalent grafting by counterion confinement.*

To test this hypothesis, we prepared a set of three platinum complexes {**Pt_1**, **Pt_2**, **Pt_{12}**} shown in **Figure 2**. These complexes, which were synthesised following published procedures,[12–14] vary in their charge from [$^{2+}$] to [$^{24+}$], yet share the same anion [BF_4^-]. This set allows us to study the dependence of surface binding on the number of anions per complex (criterion 1) and the application to complexes of various sizes. As a support, we chose Vulcan XC72 (hereafter: Vulcan) owing to its high surface area (~ 210 m^2g^{-1}) and abundant micropores (~ 15% of V_{tot}) for confining the counterions (criterion 2).[15] Moreover, the BF_4^- counterions could form stabilizing anion-π interactions with the graphitic π-systems of Vulcan (criterion 3).[16]

The surface immobilization of the complexes on Vulcan (denoted hereafter as **Pt_1**@Vulcan, **Pt_2**@Vulcan and **Pt_{12}**@Vulcan) was done using conventional wet impregnation (see details in the experimental section). In each case, we prepared samples with two Pt loadings: 5.0 and 12.5 μmol Pt g_{vulcan}^{-1}, respectively. Choosing for loading by weight rather than by molarity enables a comparison across the set, as otherwise the total number of *anions* per sample would differ by an order of magnitude (loading by weight ensures an identical number of counterions per sample). Furthermore, by preparing different loadings of each sample, we could study trends correlated with platinum loading.

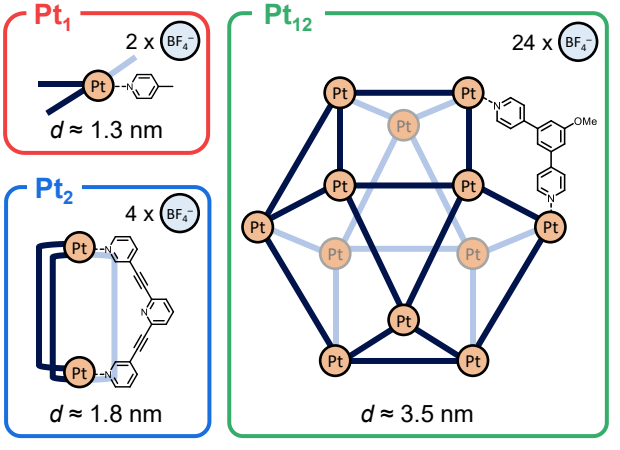

Figure 2. *Ball-and-stick model structures of the three complexes Pt_1, Pt_2 and Pt_{12}. The balls represent Pt atoms, and the sticks represent the connecting organic moieties (one of which is shown for each structure).*

Physical characterization of the immobilized complexes

The impregnated complexes were characterised by aberration corrected high-angle annular dark-field scanning transmission electron microscopy (AC-HAADF-STEM) and energy-dispersive X-ray (EDX) imaging to study the distribution of the complexes and their counterions over the Vulcan surface (**Figure 3**). Both techniques showed that the complexes and counterions were homogeneously distributed over the surface without any clustering. This means that our impregnation method ensures a direct interaction between the support and all

complexes, which is critical for combining the useful functionalities of the support and complex in designing advanced materials.

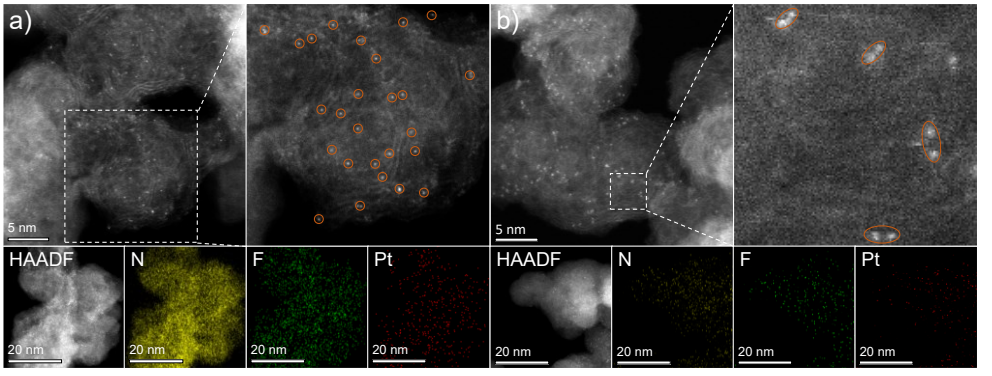

Figure 3. *AC-HAADF-STEM-EDX imaging of a) Pt_1@Vulcan and b) Pt_2@Vulcan. AC-HAADF-STEM imaging (left panels) and zoom-ins (right panels) showing single bright dots of Pt atoms as indicated by the orange circles and ovals. The EDX mapping shows the equal distribution of N, F and Pt over the surface for the samples. The variation in EDX-intensity between samples is attributed to different acquisition parameters.*

The surface area and porosity of the grafted materials were studied using N_2 adsorption at 77 K (**Figure 4** and **Figures S1-S7**). The sorption isotherms are all highly similar and show classical type II curves indicating microporous materials with cylindrical pores.[17] They do differ in two aspects: the total adsorbed volume, and the adsorbed volume at low partial pressures (**Figures 4a-c**).

These results tell us two things: First, the decrease in total adsorbed volume is in line with the respective SSAs and comes with increasing complex loading (see insets in **Figures 4a-c**). All the samples show that there is less surface area accessible for N_2 adsorption after immobilizing **Pt_1**, **Pt_2** or **Pt_{12}** on Vulcan. This cannot be explained by simply covering the surface with complexes, because the decrease in surface area is a factor of five higher than what would be expected based on the actual size of the complexes (**Table S1** and further details in the appendix). A more reasonable explanation is pore blocking by counterion confinement and/or adsorbed complexes covering pore entrances (*vide infra*). The

fact that the decrease is linear (see insets in **Figures 4a-c**) also supports the sub-monolayer dispersed adsorption of the complexes. Indeed, this is what we see also in the AC-HAADF-STEM images in **Figure 3**.

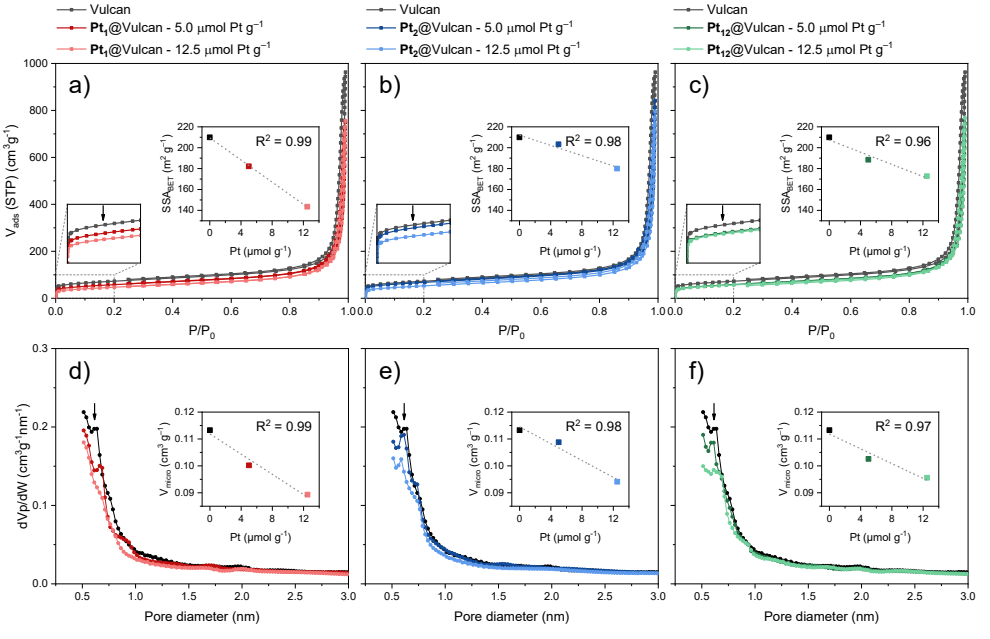

Figure 4. *Physical characterization of Pt_1@Vulcan, Pt_2@Vulcan and Pt_{12}@Vulcan at different platinum loadings by N_2 adsorption at 77 K. a-c) N_2 adsorption isotherms at 77 K. Insets show a linear fit between the specific surface area (SSA) obtained using the Brunauer-Emmett-Teller (BET) method and the platinum loading. d-f) The corresponding micropore size distributions using the Horváth-Kawazoe method. Insets show a linear fit between the total micropore volume (V_{micro}) and the platinum loading.*

Second, the steep rise at low partial pressures is less pronounced with increasing complex loadings and is seen in all three cases (see zoom-ins in **Figures 4a-c**). This indicates that fewer micropores are available for nitrogen sorption after immobilization. Looking at the micropore-size distributions (determined using the Horvath-Kawazoe method) we see a decrease in pores with a diameter of ~0.7 nm, independent of which complex is immobilized (**Figures 4d-f**). As the complexes' hydrodynamic radii are > 0.7 nm, this decrease cannot be due to confinement of the

complexes in the surface micropores. The BF_4^- counterions, however, are only ~0.3 nm in diameter, and fit well into these pores, thereby satisfying criterion 2. Moreover, the optimal distance for stabilizing anion-π interactions between the boron atom of BF_4^- and graphitic π-systems is ~0.35 nm.[16] This is exactly half of the decreasing pore diameter, indicating a perfect fit with stabilizing anion-π interactions within the cylindrical micropores, satisfying criterion 3. Finally, the average slope of the insets in **Figures 4d-f** corresponds to a volume decrease which is a factor of seven higher than what would be expected based on the actual size of BF_4^- (see details in the appendix). This is likely because BF_4^- anions remain confined at the mouth of the micropores, staying close to the cationic complex.

Adsorption kinetics and isotherms of the complexes

Next, we monitored the immobilization process of **Pt_1**, **Pt_2** and **Pt_{12}** on Vulcan over time by studying their binding kinetics (**Figure 5**). This was done by sampling at different times after the complexes were added to a well-dispersed suspension of Vulcan. Each sample was quickly filtered, and the filtrate was analysed to determine the adsorbed fraction (see **Figures S8-S13** and further details in the experimental section). For **Pt_1** (red curve in **Figure 5**) the surface coverage reached its final value (~85%) within fifteen seconds of equilibration time, indicating non-restricted and relatively weak binding (*vide infra*). The other two complexes adsorb spontaneously on the surface in a two-step process: a fast initial adsorption of a large fraction of the dissolved complexes, followed by a slow adsorption of the remaining amount. In the case of **Pt_2** (blue curve in **Figure 5**), ca. 65% of the complexes adsorbed within fifteen seconds, then the mixture remains stable for four minutes, and then the rest of the complexes adsorb slowly, within 16 h. The most striking adsorption behaviour was observed for the largest complex, **Pt_{12}** (green curve in **Figure 5**). Nearly 85% of it adsorbed within fifteen seconds, followed by a release of 20% back into solution after four minutes and a slow re-adsorption thereafter to reach complete adsorption within 16 h.

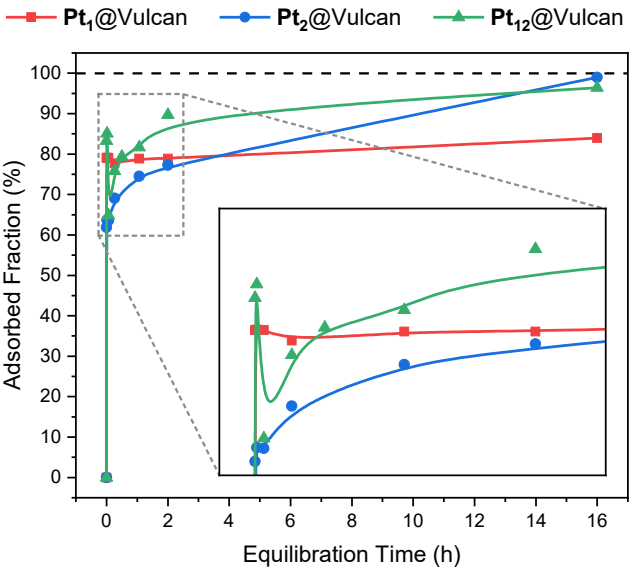

Figure 5. *Adsorption kinetics of Pt_1, Pt_2 and Pt_{12} on Vulcan.*

Based on these results, we suggest that there are two processes here, namely *surface adsorption* and *surface binding*. The former is fast, as it involves only van de Waals forces and can occur on any site on the surface. Nor does it distinguish much between types and sizes of complexes. The latter process, however, is slower and more intricate. It forms interactions that require suitable binding spots. Such a two-step mechanism, generally referred to as indirect adsorption, is much more common than the direct option, where the complex stays put at its initial point of adsorption.[18] The second step involves per definition a detachment of the complex from its initial binding site. In the case of **Pt_{12}**, that bears no less than 24 counterions, dissolution is more favoured, and therefore the lack of suitable sites leads to an intermediate net surface desorption, until each complex finds its place.

To gain further insight into the binding strength of **Pt_1**, **Pt_2** and **Pt_{12}** on Vulcan, we measured their adsorption isotherms (**Figures S14a-c**). This was done by preparing sets of samples with an equal amount of support yet using different concentrations of the complexes, starting from 7.15 µM Pt and going up to 70.71 µM (the concentration used in the adsorption kinetics experiments). After 16 h of equilibration, the samples were filtered, and the concentrations of the supernatants

were determined to quantify the adsorbed fraction (see **Figures S8-S13** and further details in the experimental section). We see that all the isotherms fit well to the solution analogue of the Brunauer-Emmett-Teller (BET) model ($R^2 > 0.996$ for eight observations).[19] **Pt_1** shows a typical C1 curve, indicating unrestricted adsorption at equal binding sites.[20] For **Pt_2** and **Pt_{12}** the curve is better described by a Langmuir-type isotherm, L3, indicating minor interactions between the adsorbed complexes. This difference is in line with the increase in the adsorbate–adsorbate binding constants for the larger complexes (**Table S2**).

Most importantly, the surface–adsorbate binding constants (K_S), **Pt_1** (5.3 M^{-1}), **Pt_2** (6.3×10^4 M^{-1}) and **Pt_{12}** (1.6×10^6 M^{-1}), increase quadratically with the number of anions per molecule (**Figure S14d**). We hypothesize that this increase is caused by cooperative binding of multiple anions to one single complex (just like with a multidentate ligand) satisfying criterion 1.[21] The value of K_S for **Pt_{12}** corresponds to a free energy of adsorption of –35 kJ mol^{-1}. This value is far beyond van der Waals or any π-interactions. It is more in the range of multiple, cooperative ionic interactions.[22]

To learn more about the adsorption of **Pt_1** and **Pt_2** on Vulcan we also determined the values of K_S during the impregnation at t = 10 min and t = 2 h (**Figures S15-S16**). For **Pt_1** we know that all adsorption happens within 15 s (red curve in **Figure 5**), and we found that K_S remained constant throughout the adsorption process (t = 10 min, 5.2 M^{-1}; t = 2 h, 5.4 M^{-1}; t = 16 h, 5.3 M^{-1}). This means that either the 2nd step of travel and binding at a vacant site already occurred for all complexes within 15 s, or that this step does not take place at all. Conversely, **Pt_2** shows a second binding process going from t = 4 min to t = 16 h (blue curve in **Figure 5**), and K_S was found to increase over time (t = 10 min, 5.6×10^4 M^{-1}; t = 2 h, 6.0×10^4 M^{-1}; t = 16 h, 6.3×10^4 M^{-1}). Thus, the average binding strength of adsorbed **Pt_2** increases during impregnation. This supports our hypothesis that the 1st step is a weak *surface adsorption,* and the 2nd step is a strong *surface binding,* which is induced by anion confinement in the micropores.

Proposed immobilization mechanism

Based on the above results, we propose a two-step immobilization mechanism (**Figure 6**): In the first, *surface adsorption* step, the complex adsorbs at a random site in a process driven by van der Waals interactions and the free energy gain of physisorption. Subsequently, it travels over the surface until it finds a suitable binding spot: a site where sufficient anions can confine in micropores close to the complex, resulting in *surface binding*.

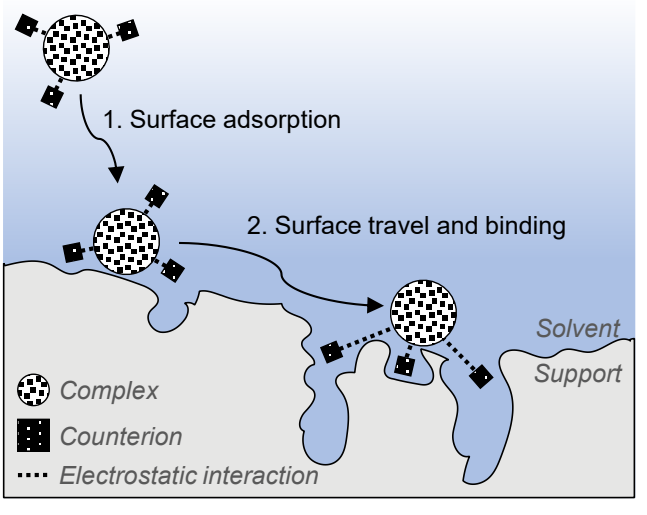

Figure 6. *Proposed immobilization mechanism of molecular complexes on charge neutral supports via adsorption and surface travel to a suitable binding site.*

Conclusions

Counterion confinement in surface pores is a simple and efficient method for non-covalent grafting of complexes to charge-neutral supports. Moreover, the method is generic, as the same counterion can be used for binding different complexes of varying charges and sizes. The process comprises two steps: adsorption at a random site, followed by surface travel and binding through counterion confinement in the micropores. Importantly, the travel across the surface promotes a homogeneous distribution of the complexes. Such a distribution is an advantage in many applications, including catalysis and molecular sensing. The final binding

strength depends on the number of counterions per complex: more counterions lead to stronger binding. Overall, this generic and simple method for binding complexes to neutral surfaces opens opportunities for making new materials that can help address today's environmental problems.

References

[1] S. Chu, Y. Cui, N. Liu, *Nat. Mater.* **2017**, *16*, 16–22.
[2] L. Li, P. C. M. Laan, X. Yan, X. Cao, M. J. Mekkering, K. Zhao, L. Ke, X. Jiang, X. Wu, L. Li, L. Xue, Z. Wang, G. Rothenberg, N. Yan, *Adv. Sci.* **2023**, *10*, 2206180.
[3] T. Keijer, T. Bouwens, J. Hessels, J. N. H. Reek, *Chem. Sci.* **2021**, *12*, 50–70.
[4] J. Biemolt, P. Jungbacker, T. van Teijlingen, N. Yan, G. Rothenberg, *Materials* **2020**, *13*, 425.
[5] G. Rothenberg, *Sust. Chem. Clim. Action* **2023**, *2*, 100012.
[6] D. S. Su, S. Perathoner, G. Centi, *Chem. Rev.* **2013**, *113*, 5782–5816.
[7] V. Georgakilas, J. A. Perman, J. Tucek, R. Zboril, *Chem. Rev.* **2015**, *115*, 4744–4822.
[8] J. Biemolt, I. M. Denekamp, T. K. Slot, G. Rothenberg, D. Eisenberg, *ChemSusChem* **2017**, *10*, 4018–4024.
[9] P. McMorn, G. J. Hutchings, *Chem. Soc. Rev.* **2004**, *33*, 108–122.
[10] J. M. Fraile, J. I. García, J. A. Mayoral, *Chem. Rev.* **2009**, *109*, 360–417.
[11] R. Anwander, in *Handbook of Heterogeneous Catalysis*, Wiley-VCH Verlag GmbH & Co. KGaA., **2008**, pp. 583–614.
[12] E. O. Bobylev, J. Ruijter, D. A. Poole III, S. Mathew, B. de Bruin, J. N. H. Reek, *Angew. Chem. Int. Ed.* **2023**, *62*, e202218162.
[13] E. O. Bobylev, D. A. Poole III, B. de Bruin, J. N. H. Reek, *Chem. Sci.* **2021**, *12*, 7696–7705.
[14] E. O. Bobylev, D. A. Poole III, B. de Bruin, J. N. H. Reek, *Chem. Eur. J.* **2021**, *27*, 12667–12674.
[15] T. Soboleva, X. Zhao, K. Malek, Z. Xie, T. Navessin, S. Holdcroft, *ACS Appl. Mater. Interfaces* **2010**, *2*, 375–384.
[16] A. Bauzá, T. J. Mooibroek, A. Frontera, *CrystEngComm* **2016**, *18*, 10–23.
[17] S. Lowell, J. E. Shields, M. A. Thomas, M. Thommes, in *Characterization of Porous Solids and Powders: Surface Area, Pore Size and Density* (Ed.: B. Scarlett), Kluwer Academic Publishers, Dordrecht, **2004**, pp. 12–14.
[18] I. Chorkendorff, J. W. Niemantsverdriet, *Concepts of Modern Catalysis and Kinetics*, Wiley-VCH Verlag GmbH & Co. KGaA., Weinheim, **2003**.
[19] A. Ebadi, J. S. Soltan Mohammadzadeh, A. Khudiev, *Adsorption* **2009**, *15*, 65–73.
[20] C. H. Giles, T. H. MacEwan, S. N. Nakhwa, D. Smith, *J. Chem. Soc.* **1960**, 3973–3993.
[21] C. A. Hunter, H. L. Anderson, *Angew. Chem. Int. Ed.* **2009**, *48*, 7488–7499.

[22] J. W. Steed, J. L. Atwood, *Supramolecular Chemistry*, Wiley-VCH Verlag GmbH & Co. KGaA., **2013**.
[23] J. Rouquerol, P. Llewellyn, F. Rouquerol, in *Studies in Surface Science and Catalysis* (Eds.: P.L. Llewellyn, F. Rodriquez-Reinoso, J. Rouqerol, N. Seaton), Elsevier, **2007**, pp. 49–56.
[24] T. Islamoglu, K. B. Idrees, F. A. Son, Z. Chen, S.-J. Lee, P. Li, O. K. Farha, *J. Mater. Chem. A* **2021**, *10*, 157–173.
[25] G. Horváth, K. Kawazoe, *J. Chem. Eng. Jpn.* **1983**, *16*, 470–475.
[26] A. Saito, H. C. Foley, *AIChE J* **1991**, *37*, 429–436.
[27] P. C. M. Laan, E. O. Bobylev, F. J. de Zwart, J. A. Vleer, A. Troglia, R. Bliem, G. Rothenberg, J. N. H. Reek, N. Yan, *Chem. Eur. J.* **2023**, in press.
[28] H. Yokoyama, Y. Ueda, D. Fujita, S. Sato, M. Fujita, *Chem. Asian J.* **2015**, *10*, 2292–2295.
[29] L. Chen, T. Yang, H. Cui, T. Cai, L. Zhang, C.-Y. Su, *J. Mater. Chem. A* **2015**, *3*, 20201–20209.

Appendix

General Considerations

All reactions were carried out in air at room temperature unless noted otherwise. To prevent cross-contamination of trace metals, all glassware used were single use scintillation vials or glassware which was cleaned with aqua regia (HNO_3:HCl 1:3 molar ratio) before use. All water used was demineralized water which was deionized by the Milli-Q technique and has a resistance greater than 18.2 MΩ·cm at room temperature. All reagents were purchased from commercial suppliers and used as received unless mentioned otherwise. Specifically, Vulcan XC72 was obtained from Cabot and acetonitrile (99.9%, Extra Dry over Molecular Sieve, AcroSeal) was obtained from Fisher Scientific B.V. The self-assembled supramolecular structures $Pt_1L_4(BF_4)_2$ (**Pt_1**, L = *p*-picoline)[12], $Pt_2L_4(BF_4)_4$ (**Pt_2**, L = 2,6-bis(pyridine-3-ylethynyl)pyridine)[13] and $Pt_{12}L_{24}(BF_4)_{24}$ (**Pt_{12}**, L = 4,4'-(5-methoxy-1,3-phenylene)dipyridine)[14] were synthesized according to literature procedures. **Pt_1** was stored as a solid and **Pt_2** and **Pt_{12}** were stored as solutions (5.0 mM Pt) in MeCN in J Young Schlenk flasks at 5 °C.

Instrumentation and characterization methods

N_2 adsorption–desorption isotherms were measured on a Thermo Scientific Surfer instrument at 77 K, using vacuum-dried samples. More specific, around 100 mg of

each sample was dried at 100°C for 16 h on a Belprep-vacIII prior to analysis. The specific surface area was determined based on the adsorption branch and the BET analysis was performed according to the Rouquerol consistency criteria.[17,23,24] All samples satisfied the four Rouquerol criteria (**Figures S1-S7**). The pore size distributions were determined based on the adsorption branch of the isotherm using the Horvath-Kawazoe (HK) technique[25] including the additions of Saito and Foley.[26]

Aberration-corrected high angle annular dark-field scanning transmission electron microscopy (AC-HAADF-STEM) measurements, elemental mappings, and energy-dispersive X-ray spectroscopy (EDS) measurements were taken on a ThermoFisher Scientific FEI Themis Z instrument coupled with a high-angle annular dark field (HAADF) detector and an energy-dispersive X-ray spectroscopy detector. The samples were deposited on a Holey carbon coated TEM-grid (300 mesh Cu grid, Pacific Grid Tech, USA). The set-up was operated at 200kV and delivers a spatial resolution of ≤70 pm in both TEM and STEM resulting in atomic-resolution imaging of the samples.

UV-Vis spectra were obtained on a double beam Shimadzu UV-2600 spectrometer at room temperature using quartz cuvettes with a path length of 2 or 10 mm and clean solvent as a background. Spectra were obtained between 225 and 500 nm using a spectral bandwidth of 0.5 nm. After data acquisition, the spectra were zeroed at 500 nm.

Surface immobilization

The self-assembled supramolecular structures **Pt_1**, **Pt_2**, and **Pt_{12}** were immobilized following a published procedure.[27] In short, Vulcan (150 mg) was finely dispersed as a black suspension in acetonitrile (11.25 mL (for 5.0 µmol Pt g_{vulcan}^{-1}) or 9.00 (for 12.5 µmol Pt g_{vulcan}^{-1})) by ultrasonication in a 100 mL round bottom flask for 1 h. Then, an acetonitrile solution of the respective organometallic complex (1.5 mL, 0.5 mM Pt, 0.75 µmol Pt (for 5.0 µmol Pt g_{vulcan}^{-1})) or 3.75 mL, 0.5 mM Pt, 1.875 µmol Pt (for 12.5 µmol Pt g_{vulcan}^{-1})) was added dropwise to the Vulcan suspension over the course of 3 h under vigorous stirring. After complete addition, the reaction mixture was left to stir at room temperature for an additional 16 h. Thereafter,

acetonitrile was removed *in vacuo* over the course of 1 h. The remaining black powder was further dried under vacuum (5 mbar at 50 °C) for 16 h and named **Pt_1**@Vulcan, **Pt_2**@Vulcan, and **Pt_{12}**@Vulcan**,** respectively.

Adsorption kinetics

The adsorption kinetics of **Pt_1**, **Pt_2**, and **Pt_{12}** on the heterogeneous support Vulcan was followed over time by UV-Vis spectroscopy via the solution depletion method. The ratios between support, solvent and the adsorbate were kept identical to these as used during cage immobilization (5.0 µmol Pt g_{vulcan}^{-1}). Thus, Vulcan (286 mg) was finely dispersed as a black suspension in acetonitrile (19.71 mL) by ultrasonication in a 100 mL round bottom flask for 1 h. Then, an acetonitrile solution of **Pt_1**, **Pt_2**, or **Pt_{12}** (286 µL, 5.0 mM Pt, 1.43 µmol Pt) was added instantaneously to the Vulcan suspension under vigorous stirring. While the reaction mixture was left to stir at room temperature for 16 h, eight samples (1.5 mL of the suspension) were taken at 15 s, 1 min, 4 min, 16 min, 64 min, 2 h and 16 h. After filtration of the suspension over a 0.45 µm filter, the filtrates were analysed by UV-Vis spectroscopy. The decrease in adsorption was attributed to immobilization of the molecular species on the heterogeneous support Vulcan. The remaining concentration of the molecular species samples in the filtrates was determined using their respective UV-Vis calibration curves (**Figures S8-S13**).

Adsorption isotherms

The adsorption isotherms of **Pt_1**, **Pt_2**, and **Pt_{12}** on the heterogeneous support Vulcan were determined by UV-Vis spectroscopy via the solution depletion method using eight different concentrations. Vulcan (57.2 mg) was finely dispersed as a black suspension in acetonitrile (3.440 – 3.942 mL) by ultrasonication in a 15 mL centrifuge tube for 1 h. Then, acetonitrile solutions (0.5 mM Pt) of **Pt_1**, **Pt_2**, or **Pt_{12}** (0.560, 0.280, 0.215, 0.166, 0.127, 0.098, 0.075 and 0.058 mL) were added instantaneously to the Vulcan suspensions so that the total volume in all samples was equal (4.00 mL). The samples were equilibrated using a temperature controlled shaking water bath (Julabo SW23) at 200 rpm at 22 °C for 10 min, 2h or 16 h. Afterwards, the samples were centrifuged (5000 rpm for 10 min) resulting in a black residue and a yellow to colourless supernatant which was analysed by UV-Vis

spectroscopy. The decrease in adsorption was attributed to immobilization of the molecular species on the heterogeneous support Vulcan. The remaining concentration of the molecular species samples in the filtrates was determined using their respective UV-Vis calibration curves (**Figures S8-S13**). The adsorption data was fitted to the solution analogue of the Brunauer–Emmett–Teller model using Origin 2018 (**Eq. S1**).[19]

$$\theta = \theta_{max} \left(\frac{K_S c}{(1 - K_L c)(1 - K_L c + K_S c)} \right) \quad \text{(S1)}$$

In which θ = total surface coverage in $\mu mol_{adsorbate}\ g_{Vulcan}^{-1}$, θ_{max} = monolayer surface coverage in $\mu mol_{adsorbate}\ g_{Vulcan}^{-1}$, K_S = surface-adsorbate binding constant in M^{-1}, K_L = adsorbate-adsorbate binding constant in M^{-1} and c = equilibrium adsorbate concentration in M.

Nitrogen adsorption – desorption studies: Rouquerol analyses

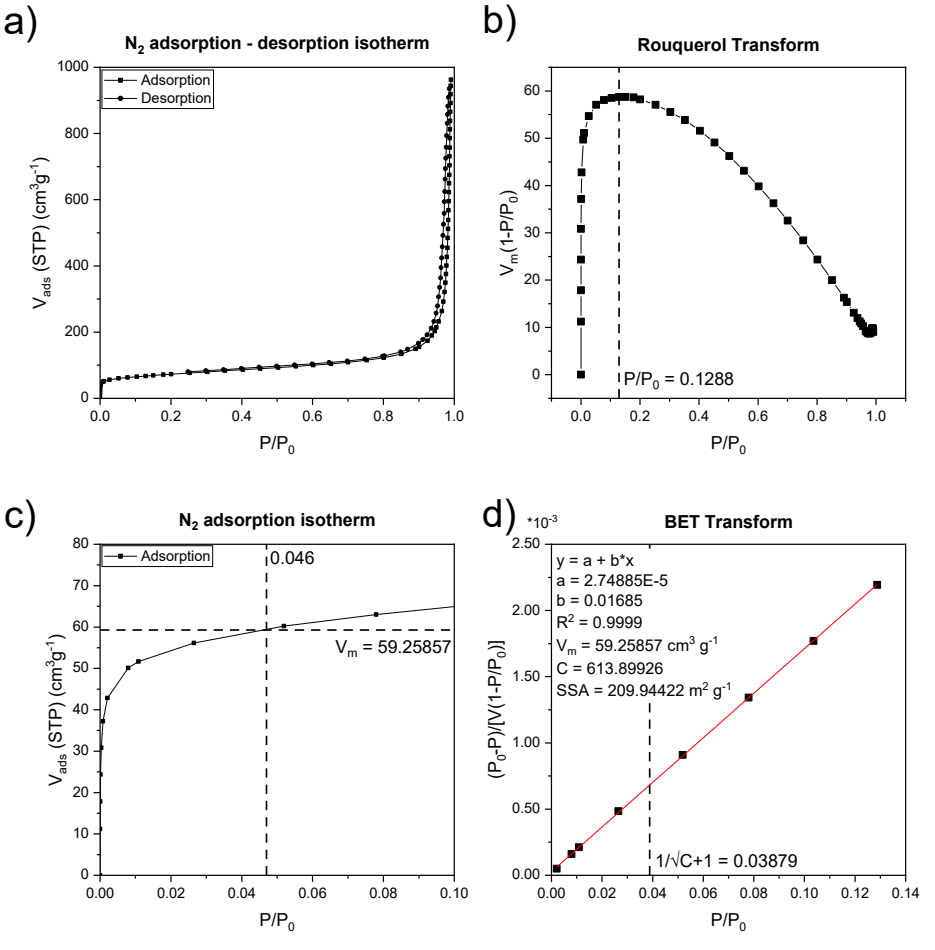

Figure S1. Porosity analysis of Vulcan. a) N_2 adsorption and desorption isotherms at 77 K; b) Rouquerol transform plot; c) zoom-in of the N_2 adsorption isotherm at 77 K and d) BET transform plot.

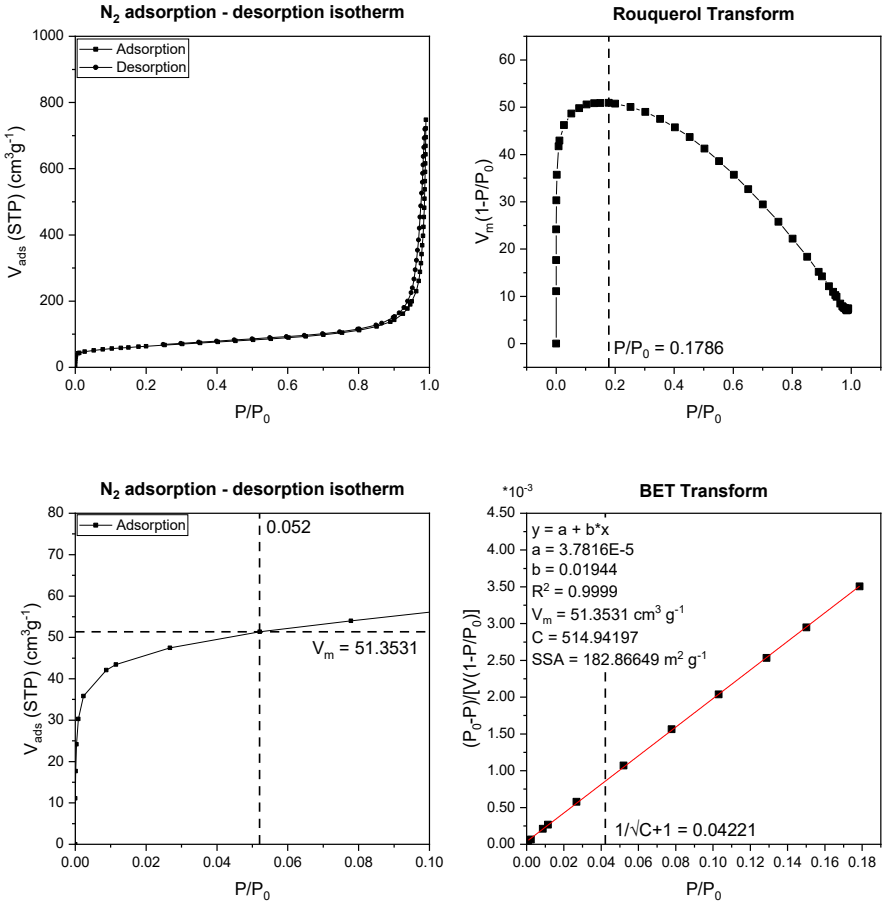

Figure S2. Porosity analysis of **Pt_1**@Vulcan (5.0 μmol Pt g_{vulcan}^{-1}). a) N_2 adsorption and desorption isotherms at 77 K; b) Rouquerol transform plot; c) zoom-in of the N_2 adsorption isotherm at 77 K and d) BET transform plot.

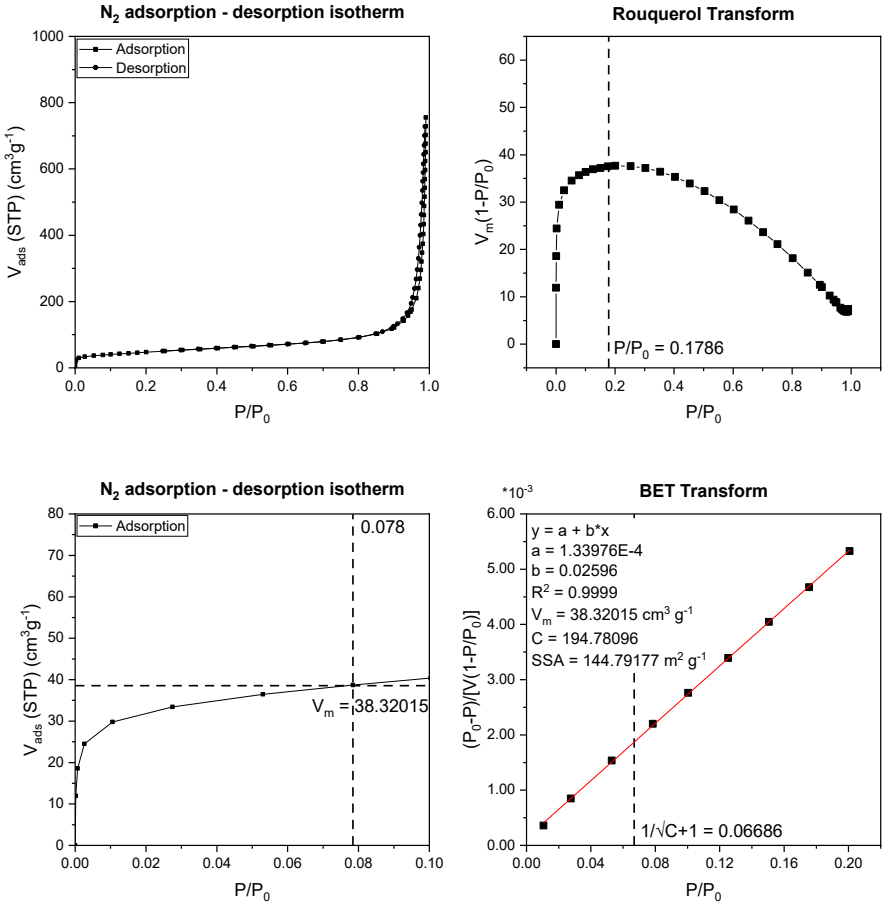

Figure S3. Porosity analysis of **Pt_1**@Vulcan (12.5 μmol Pt g_{vulcan}^{-1}). a) N_2 adsorption and desorption isotherms at 77 K; b) Rouquerol transform plot; c) zoom-in of the N_2 adsorption isotherm at 77 K and d) BET transform plot.

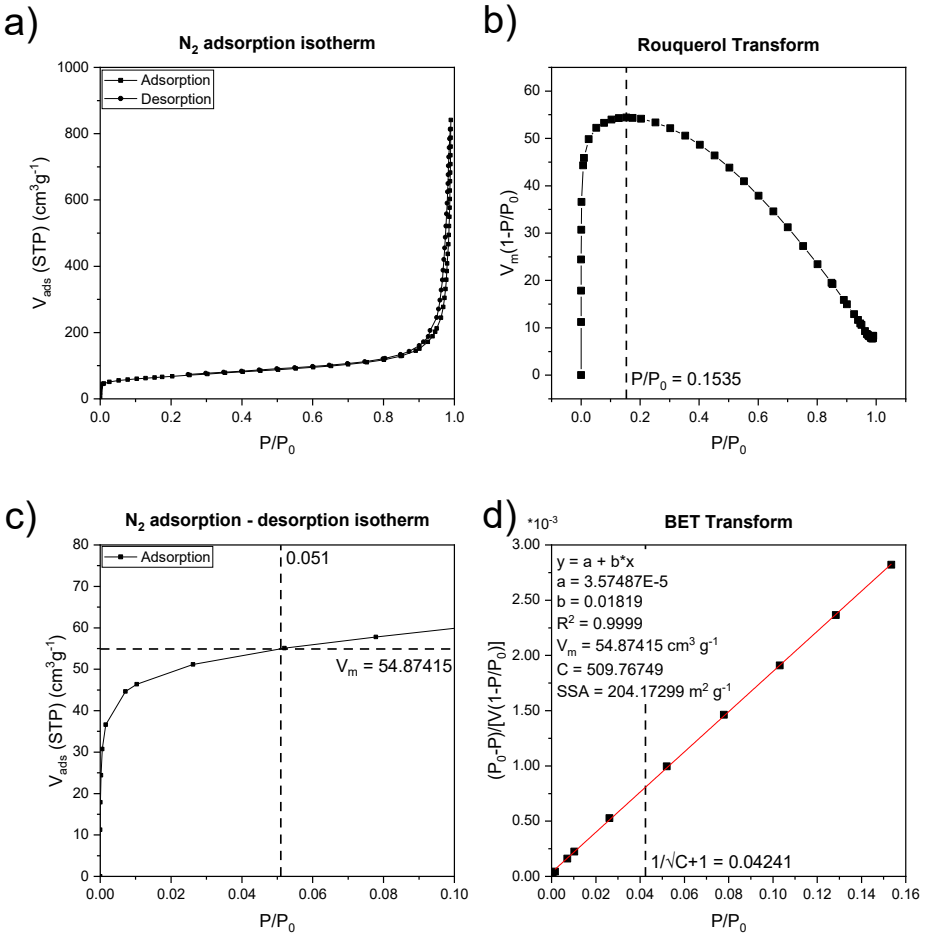

Figure S4. Porosity analysis of **Pt_2**@Vulcan (5.0 μmol Pt g_{vulcan}^{-1}). a) N_2 adsorption and desorption isotherms at 77 K; b) Rouquerol transform plot; c) zoom-in of the N_2 adsorption isotherm at 77 K and d) BET transform plot.

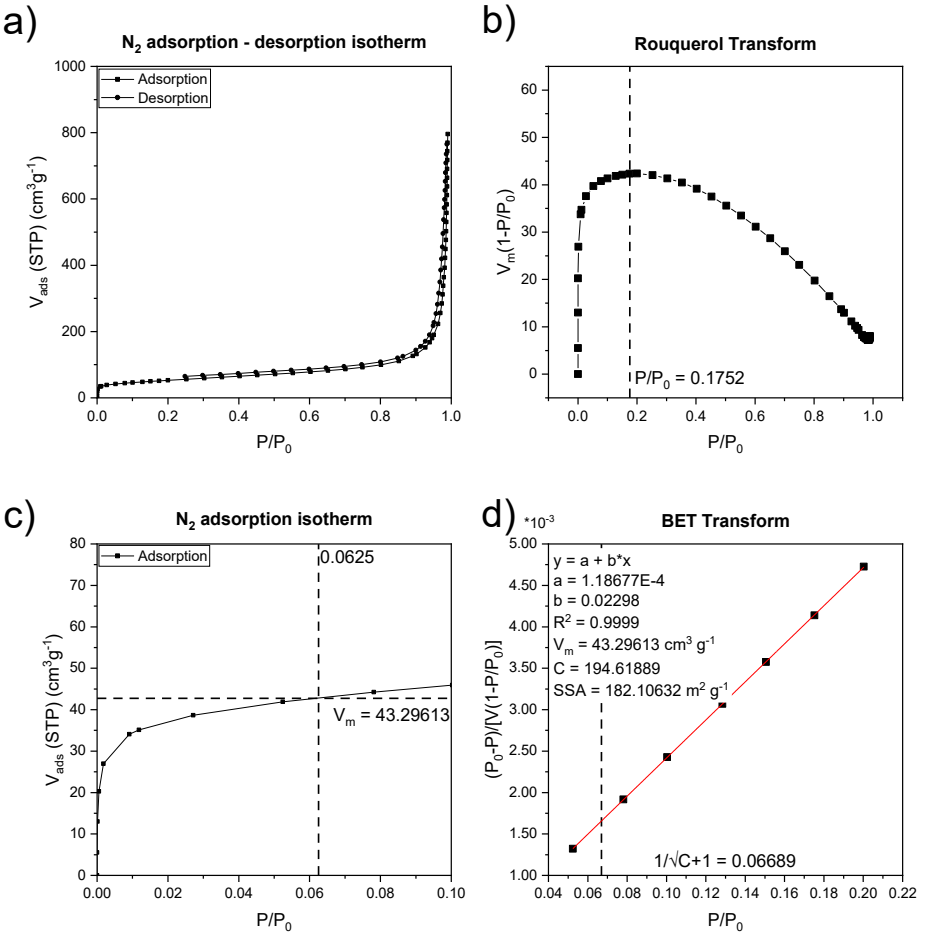

Figure S5. Porosity analysis of **Pt_2**@Vulcan (12.5 μmol Pt g_{vulcan}^{-1}). a) N_2 adsorption and desorption isotherms at 77 K; b) Rouquerol transform plot; c) zoom-in of the N_2 adsorption isotherm at 77 K and d) BET transform plot.

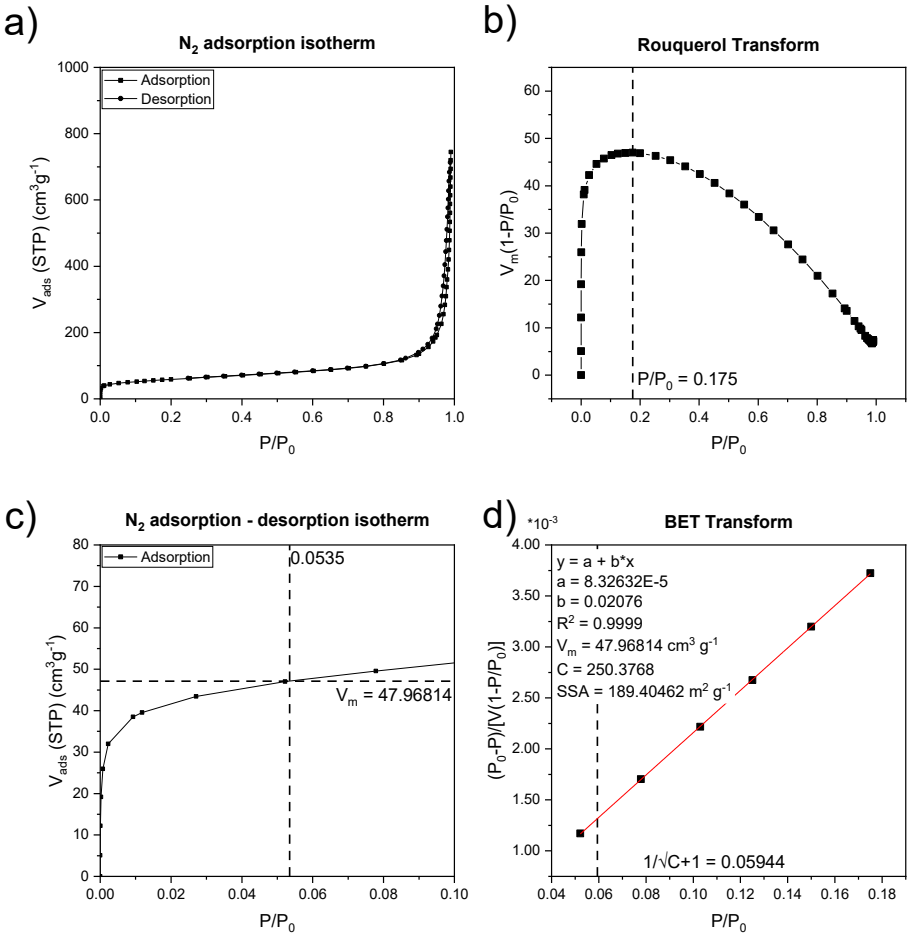

Figure S6. Porosity analysis of **Pt_{12}**@Vulcan (5.0 μmol Pt g_{vulcan}^{-1}). a) N_2 adsorption and desorption isotherms at 77 K; b) Rouquerol transform plot; c) zoom-in of the N_2 adsorption isotherm at 77 K and d) BET transform plot.

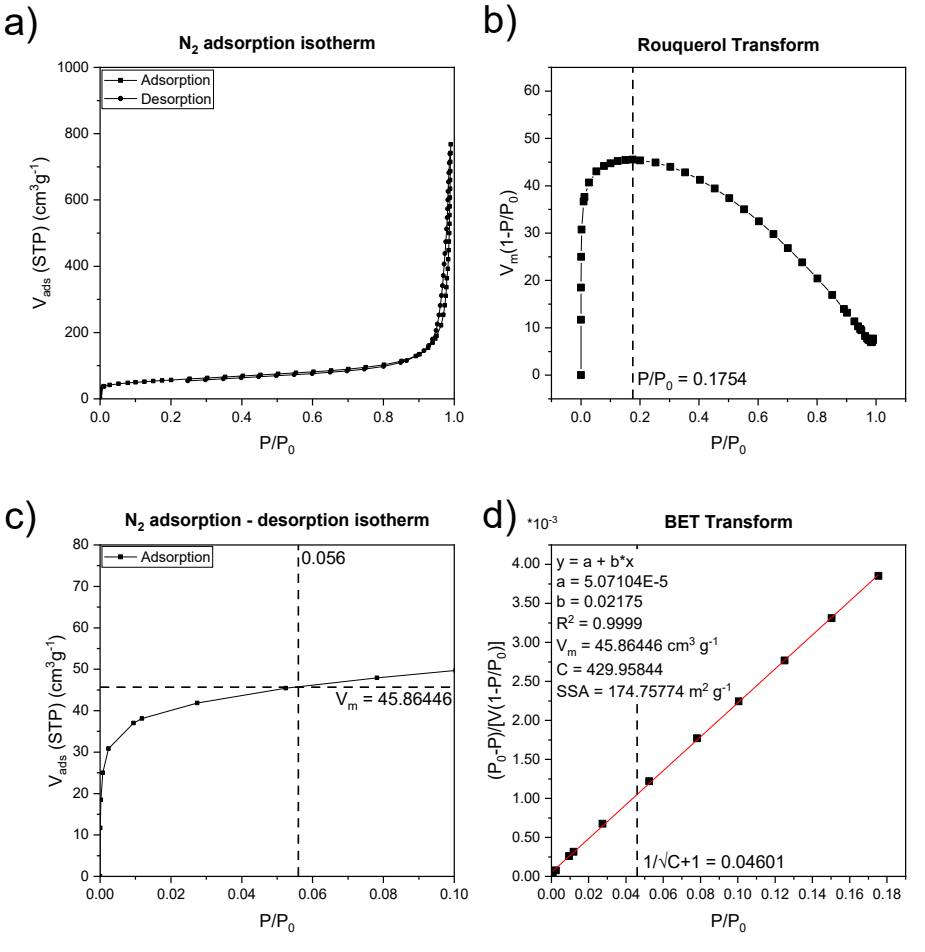

Figure S7. Porosity analysis of **Pt_{12}**@Vulcan (12.5 μmol Pt g_{vulcan}^{-1}). a) N_2 adsorption and desorption isotherms at 77 K; b) Rouquerol transform plot; c) zoom-in of the N_2 adsorption isotherm at 77 K and d) BET transform plot.

UV-Vis calibration curves

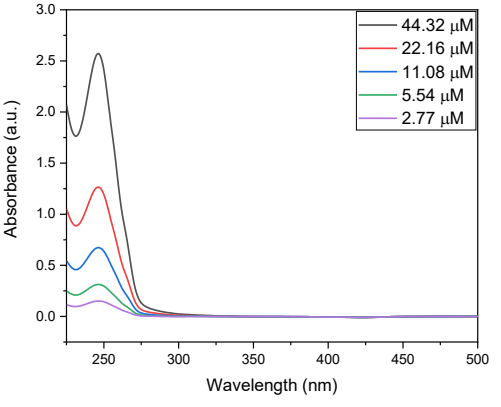

Figure S8. UV-Vis spectra of **Pt_1** in MeCN in the concentration range 2.77 – 44.32 µM measured in a cuvette with a path length of 10 mm.

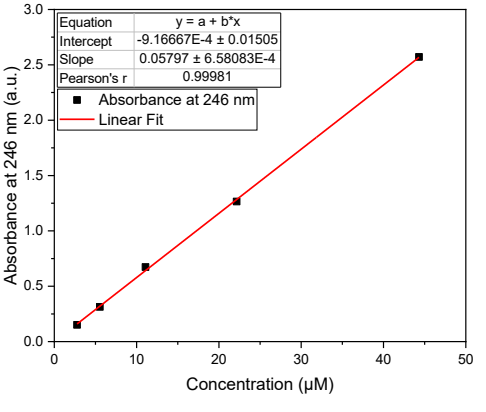

Figure S9. Lambert-Beer plot of **Pt_1** in MeCN in the concentration range 2.77 – 44.32 µM measured in a cuvette with a path length of 10 mm: λ_{max}/nm (ε/L mol^{-1} cm^{-1}): 246 (58000).

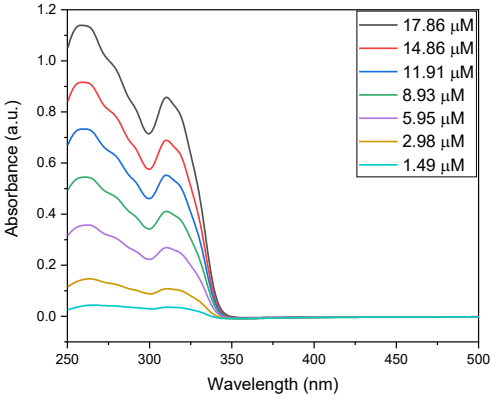

Figure S10. UV-Vis spectra of **Pt_2** in MeCN in the concentration range 1.49 – 17.86 µM measured in a cuvette with a path length of 2 mm.

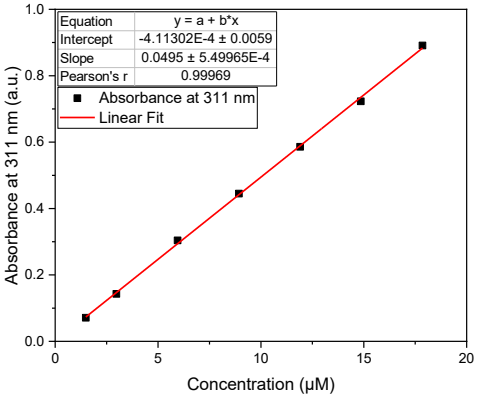

Figure S11. Lambert-Beer plot of **Pt_2** in MeCN in the concentration range 1.49 – 17.86 µM measured in a cuvette with a path length of 2 mm: λ_{max}/nm (ε/L mol^{-1} cm^{-1}): 311 (247500).

.

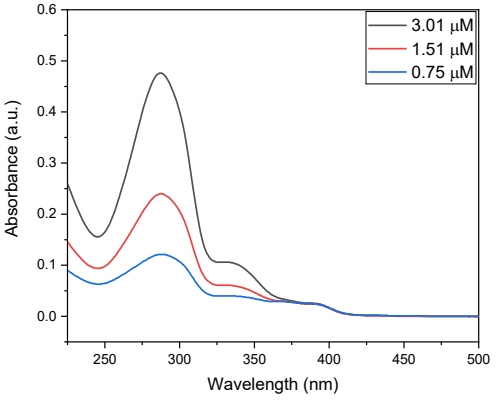

Figure S12. UV-Vis spectra of **Pt_{12}** in MeCN in the concentration range 0.75 – 3.01 µM measured in a cuvette with a path length of 2 mm.

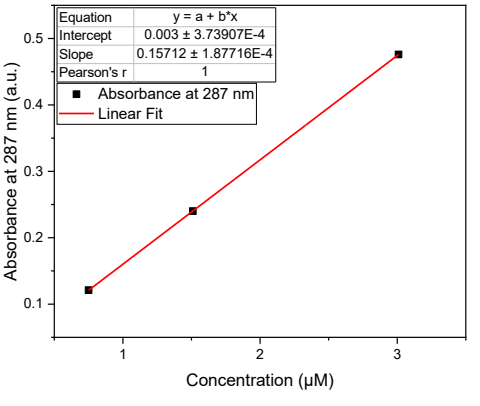

Figure S13. Lambert-Beer plot of **Pt_{12}** in MeCN in the concentration range 0.75 – 3.01 µM measured in a cuvette with a path length of 2 mm: λ_{max}/nm (ε/L mol^{-1} cm^{-1}): 287 (785600).

Additional calculations

Decrease in specific surface area (SSA)

The slope, *ΔSSA*, of the insets in **Figure 4a-c** have a unit that is described in **Eq. S2**.

$$\frac{\Delta y}{\Delta x} = \frac{[m^2 g^{-1}]}{[\mu mol_{Pt}\ g^{-1}]} = \frac{[m^2]}{[\mu mol_{Pt}]} \quad (S2)$$

This unit can be rewritten to (nm^2 $complex^{-1}$) as described in **Eq. S3** because 1 m^2 = 1*10^{18} nm^2, x number of Pt atoms = 1 complex (x = 1, 2 or 12 for **Pt_1**, **Pt_2** and **Pt_{12}**), 1 µmol = 1*10^{-6} mol and 1 mol Pt = N_A Pt atoms (N_A = 6.0221408*10^{23}).

$$Decreasing\ Area\ (nm^2 complex^{-1}) = |\Delta SSA| * \frac{10^{18} * number\ of\ Pt\ atoms\ in\ complex}{10^{-6} * N_A} \quad (S3)$$

The surface area that one molecule could cover was estimated based on X-ray structures of **Pt_1**[27], **Pt_2**[27] and **Pt_{12}**[28]. The measured diameters are listed in **Table S1**. In the case of **Pt_{12}**, an X-ray structure of an isostructural cage was used because an X-ray structure of this cage is not reported to date. The diameter of the complexes was used to calculate the area that it could cover as described in **Eq. S4**.

$$Covering\ Area\ (nm^2 complex^{-1}) = \pi * \left(\frac{d_{complex}\ [nm]}{2}\right)^2 \quad (S4)$$

This gives covering area's that are ~5 times lower than the observed decrease in surface area (**Table S1**). Note: N_2 adsorption of the complexes itself is not considered here as M_2L_4 cage structures like **Pt_2** are known to have negligible affinity for N_2 adsorption themselves.[29]

Complex	ΔSSA (m^2 μmol_{Pt}^{-1})	Decreasing Area (nm^2 $_{complex}^{-1}$)	$d_{complex}$ (nm)[27,28]	Covering Area (nm^2 $_{complex}^{-1}$)	Decreasing Area / Covering Area
Pt_1	-5.31	8.8	1.34	1.41	6.2
Pt_2	-2.45	8.1	1.80	2.54	3.2
Pt_{12}	-2.91	58.0	3.47	9.46	6.1

Table S1. Structural parameters of the complexes.

Decrease in micropore volume (V_{micro})

The slope, ΔV_{micro}, of the insets in **Figure 4d-f** have a unit that is described in **Eq. S5**.

$$\frac{\Delta y}{\Delta x} = \frac{[cm^3 g^{-1}]}{[\mu mol_{Pt}\ g^{-1}]} = \frac{[cm^3]}{[\mu mol_{Pt}]} \quad \text{(S5)}$$

This unit can be rewritten to (nm^3 BF_4 $anion^{-1}$) as described in **Eq. S6** because 1 cm^3 = $1*10^{21}$ nm^3, 1 µmol = $1*10^{-6}$ mol, 1 mol Pt = N_A Pt atoms (N_A = $6.0221408*10^{23}$) and 1 Pt atom = 2 BF_4 anions.

$$Decreasing\ Volume\ (nm^3\ BF_4\ anioin^{-1}) = |\Delta V_{micro}| * \frac{10^{21}}{2 * 10^{-6} * N_A} \quad \text{(S6)}$$

Taking the average slope, 0.00156 cm_3 mol_{Pt}^{-1}, results in an average decreased volume of 1.30 nm^3 BF_4 per anion.

The volume that one BF_4 anion would occupy can be estimated best based on its average diameter while having anion-π interactions, that is ~0.35 nm,[16] using the formula described in **Eq. S7**.

$$Occupying\ Area\ (nm^3\ BF_4\ anioin^{-1}) = \frac{4}{3} * \pi * \left(\frac{d_{complex}\ [nm]}{2}\right)^3 \quad \text{(S7)}$$

This gives an estimated occupied area by one BF_4 anion equal to 0.18 nm^3, a value that is ~7 times lower than the observed volume decrease.

Adsorption isotherms

Complex	Adsorbate–adsorbate binding constants (M^{-1})
Pt_1	$6.4x10^2$
Pt_2	$1.1x10^4$
Pt_{12}	$1.1x10^5$

Table S2. Adsorbate–adsorbate binding constants of the complexes on Vulcan, t = 16 h.

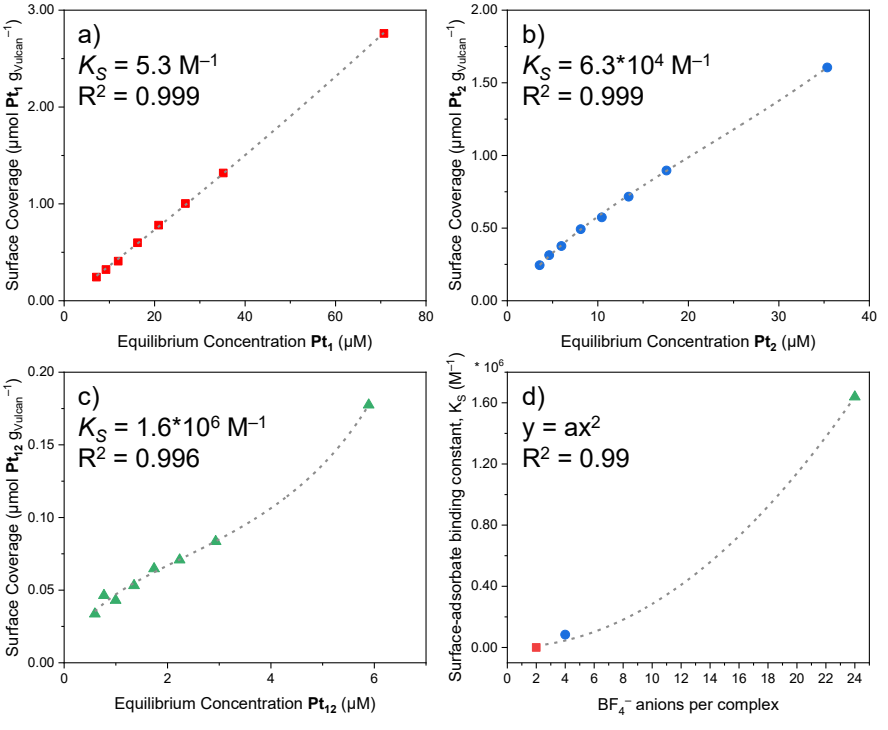

Figure S14. Adsorption isotherms of Pt_1, Pt_2 and Pt_{12} on Vulcan. a-c) Adsorption isotherms and the corresponding fitting of the solution analogue of the Brunauer–Emmett–Teller model and d) determined surface-adsorbate binding constants K_S as a function of the number of BF_4^- anions per complex and the corresponding second order polynomial fit.

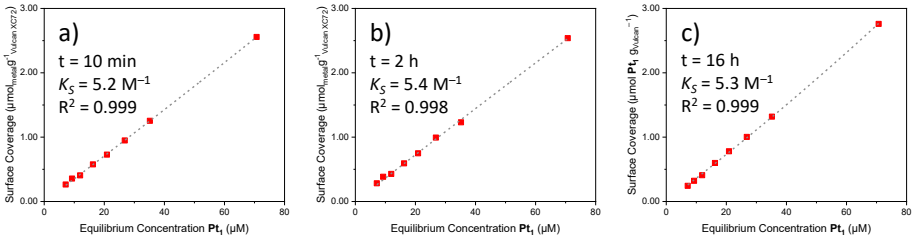

Figure S15. Adsorption isotherms of **Pt_1** on Vulcan. Adsorption isotherms and the corresponding fitting of the solution analogue of the Brunauer–Emmett–Teller model after a) 10 min, b) 2 h and c) 16h of equilibration time.

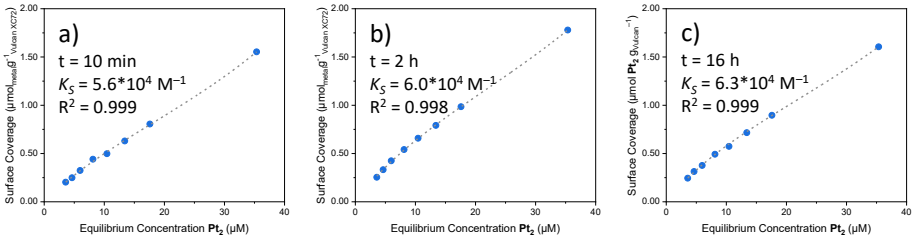

Figure S16. Adsorption isotherms of **Pt_2** on Vulcan. Adsorption isotherms and the corresponding fitting of the solution analogue of the Brunauer–Emmett–Teller model after a) 10 min, b) 2 h and c) 16h of equilibration time.